Materials Science & Engineering C 121 (2021) 111857

Contents lists available at ScienceDirect

Materials Science & Engineering C

journal homepage: www.elsevier.com/locate/msec

In vitro analysis of a physiological strain sensor formulated from a PEDOT:PSS functionalized carbon nanotube-poly(glycerol sebacate urethane) composite

Ghazal Tadayyon [a,b], Katarzyna Krukiewicz [a,c], James Britton [a], Aitor Larrañaga [a], Catalina Vallejo-Giraldo [a,d], Marc Fernandez-Yague [a], Yina Guo [e], Gemma Orpella-Aceret [a], Lu Li [a], Anup Poudel [a], Manus J.P. Biggs [a,*]

[a] Centre for Research in Medical Devices, National University of Ireland, Galway, Ireland
[b] Department of Mechanical & Manufacturing Engineering, Trinity College Dublin, University of Dublin, Ireland
[c] Department of Physical Chemistry and Technology of Polymers, Silesian University of Technology, Gliwice, Poland
[d] Department of Bioengineering, Imperial College London, London, United Kingdom
[e] Bernal Institute, University of Limerick, Limerick, Ireland

ARTICLE INFO

Keywords:
Biodegradable polymer
Strain sensor
Carbon nanotubes
PEDOT
Poly(glycerol sebacate urethane)

ABSTRACT

Biodegradable strain sensors able to undergo controlled degradation following implantation have recently received significant interest as novel approaches to detect pathological tissue swelling or non-physiological stresses. In this study, the physicomechanical, electrochemical and active pressure sensing behavior of an electrically conductive and biodegradable poly(glycerol sebacate urethane) (PGSU) composite, reinforced with poly(3,4-ethylenedioxythiophene) polystyrene sulfonate (PEDOT:PSS) functionalized carbon nanotubes (CNTs), was evaluated *in vitro*. Analysis of these PGSU-CNTs composites demonstrated that the incorporation of functionalized CNTs into a biodegradable elastomer resulted in enhanced mechanical strength, conductivity and tailored matrix biodegradation. PGSU-CNT composites were subsequently formulated into flexible and active pressure sensors which demonstrated optimal sensitivity to applied 1% uniaxial tensile strains. Finally, cytocompatibility analysis a with primary neural culture confirmed that PGSU-CNT composites exhibited low cytotoxicity, and supported neuron adhesion, viability, and proliferation *in vitro*.

1. Introduction

Biodegradable electronics, which resorb or degrade at a controlled rate following implantation, have recently come to the forefront of biomaterials research. Such materials should present biocompatibility on implantation, undergo controlled degradation, present biomimetic mechanical properties and a high level of electrical conductivity [1–6]. With respect to the development of implantable biodegradable devices, common polymers such as poly(vinyl alcohol), polycaprolactone and poly(lactic-*co*-glycolic acid), have been explored as dielectric substrates onto which printed metallic circuits can be applied to fabricate electrically active devices [7,8]. Critically, novel electrically active bioresorbable polymers with stable electrochemical properties are necessary for the development of resorbable polymer-derived flexible bioelectronics and neural interfaces [9,10].

The electrical properties of resorbable polymers can be modified extensively through the incorporation of conducting nanomaterials [11,12]. In particular, carbonaceous materials such as carbon fibers, carbon nanotubes, and graphene have been demonstrated to provide an electrical percolation pathway which grants robust electrical routing in the polymer matrices to permit conductivity [12–17]. Near the electrical percolation threshold, deformation of piezoresistive composites yields improved strain sensitivity as the structural changes in conducting networks induces noticeable changes in the composite electrical resistivity.

Owing to their superior mechanical characteristics (mechanically compliant, flexibility, torquability, and stretchability), electrically active elastomeric composites have shown great promise in many biosensing applications, including but not limited to deformation sensors [18–20], temperature sensors, and physiological sensors for therapeutic

* Corresponding author.
E-mail address: manus.biggs@nuigalway.ie (M.J.P. Biggs).

https://doi.org/10.1016/j.msec.2020.111857
Received 31 October 2020; Received in revised form 5 December 2020; Accepted 24 December 2020
Available online 6 January 2021

and diagnostic applications [21,22]. In particular recent advances in the design of stretchable and resorbable nanocomposite materials have facilitated the development of transient piezoresistive strain sensors [20,23–25].

Poly(glycerol-sebacate) (PGS) is a biocompatible and biodegradable elastomer [26] which has generated great interest as an organic material in tissue engineering applications since it was first reported in 2002 [27–31]. PGS can be synthesized from glycerol, a basic building block of lipids, and sebacic acid, a metabolic intermediate of fatty acids, *via* a two-step polycondensation/crosslinking synthesis process [26]. The mechanical properties of PGS however, can only be tailored within a narrow range (Young's modulus from 0.25 to 1.45 MPa for materials which can elongate above 100%) [32,33], in addition PGS synthesis must be performed under high temperatures (110–160 °C) and under vacuum for 2–4 days [33–35]. Recently, it has been shown that modification of the PGS structure by reacting isocyanate with the hydroxyl groups of the pre-PGS chemistry to form poly(glycerol sebacate urethane) (PGSU) offers enhanced mechanical performance and controlled degradation with retained biocompatibility [36,37]. The applicability of PGSU in soft tissue engineering has been described previously [36,37] [38] indicating that PGSU is a versatile, but underutilized biomaterial in bioelectronic applications.

In this study, the formulation of an elastomeric PGSU nanocomposite through the incorporation of poly(3,4-ethylenedioxythiophene) polystyrene sulfonate (PEDOT:PSS) functionalized carbon nanotubes (CNTs) is reported. Resulting PGSU-CNTs nanocomposite formulations were elastomeric with marked electrical conductivity and neural cytocompatibility. Furthermore, PGSU-CNTs nanocomposites were fabricated into thin-film bioresorbable strain sensors and the sensitivity and functional lifetime of these devices were assessed under simulated physiological conditions.

2. Materials and methods

2.1. Materials

Multi-walled carbon nanotubes (CNTs) (purity>98% carbon basis) with an outer diameter 10 ± 1 nm, internal diameter of 4.5 ± 0.5 nm, length 3–6 μm and aspect ratio >250–550, poly(allylamine hydrochloride) (PAH) average Mw ~ 58,000, poly(3,4-ethylenedioxythiophene) polystyrene sulfonate (PEDOT:PSS), sodium chloride (≥99.5%), glycerol (>99%), sebacic acid (99%), hexamethylene diisocyanate (HDI,99%), stannous 2-ethyl-hexanoate (95%), dimethylformamide (DMF,anhydrous,99.8%), phosphate buffered saline (PBS) tablets were purchased from Sigma-Aldrich.

2.2. Functionalization and characterization of CNTs

Carbon nanotubes were modified *via* a layer-by-layer method. First, 25 mg of poly(allylamine hydrochloride) (PAH) was dissolved in 5 ml of a 0.5 M sodium chloride aqueous solution and the pH of the resulting solution was adjusted to 6.5. Then, 5 mg of carbon nanotubes was suspended in the resulting PAH-brine solution, ultrasonicated for 1 h (SONICS Sonicator, 40% amplitude, 3.5 MJ, pulsing: 5 s on and 2 s off) and collected *via* centrifugation (Thermo Scientific HERAEUS FRESCO 17 Centrifuge, 14,000 rpm). The supernatant was subsequently removed and CNTs were resuspended and washed in a 0.5 M sodium chloride aqueous solution three times. CNTs dispersed in a 0.5 M sodium chloride aqueous solution were added dropwise to a 2.5 mg/ml PEDOT:PSS solution and ultrasonicated (SONICS Sonicator, 40% amplitude, 3.5 MJ, pulsing: 5 s on and 2 s off) for 1 h followed by centrifugation and triple washing in a 0.5 M sodium chloride aqueous solution.

The zeta potential of 0.001 mg of pristine, PAH and PAH-PEDOT:PSS functionalized CNTs was subsequently measured (a minimum of ten runs) in 1 ml of water (Malvern Instruments NanoZS90 Zetasizer). FTIR spectra of pristine and PAH functionalized CNTs were also recorded (Agilent Varian 660-IR FTIR Spectrometer) performing a total of four scans with 2 cm^{-1} resolution, in the 4000–600 cm^{-1} spectral region.

Pristine and functionalized CNTs were subjected to thermo gravimetric analysis (TGA) at a rate of 10 °C/min in air (Universal V4.3A TA instruments). 10–15 mg of pristine and functionalized CNTs were placed in platinum pans and heated from room temperature to 600 °C within a thermogravimetric analyzer (TGA Q50–0545, TA Instruments), at a heating rate of 10 °C/min and a nitrogen flux of 60 mL/min. During this process, heat flow, sample temperature, sample weight and its time derivative were recorded continuously.

TEM samples were prepared by placing the CNT suspension onto lacey carbon grids and air drying at room temperature. The size and structure of pristine, and functionalized CNTs was evaluated by high-resolution transmission electron microscopy (JEOL JEM 1200 EX), using an accelerating voltage of 200 kV.

2.3. Synthesis and characterization of PGSU-CNTs nanocomposites

PGSU synthesis was performed as previously described [26,36,39]. All polymer synthesis reactions and solvent removal processes were carried out in a well-ventilated hood with use of appropriate PPE. In brief, a pre-polymer was obtained through a condensation reaction between equimolar amount of glycerol and sebacic acid (0.05 mol) which was stirred under flowed nitrogen for 8 h at 120 °C in an oil bath. The nitrogen purge was running constantly throughout the reaction to facilitate the removal of water vapor. This step was followed by maintenance under the 3.5 mbar vacuum for 16 h. After cooling to 55 °C, the resulting yellow viscous pre-PGS was dissolved *via* sonication (SONICS Sonicator, 40% amplitude, 3.5 MJ, 3 min) in 130 ml of DMF and 0.27 ml of the catalyst (stannous 2-ethyl-hexanoate (Tin (II)), 0.05% w/v) and 8 ml of a crosslinking agent HDI (HDI:glycerol-1:1) were added to the pre-polymer solution drop by drop. The polymerization reaction was performed under nitrogen flow in an oil bath maintained at 55 °C for 2 h.

Nanocomposites of 0.5, 1, 2, 4 and 5 wt% of PAH-PEDOT:PSS functionalized CNTs were prepared in DMF and ultrasonicated (SONICS Sonicator, 40% amplitude, 3.5 MJ) for 1 h. The mixtures were then cast onto a glass petri dish and maintained at room temperature for three days. Subsequently, the composites were maintained in a vacuum oven with 3.5 mbar at 30 °C for two days. To eliminate the non-crosslinked constituents, the dry films were soaked in absolute ethanol for 24 h at room temperature and further dried in a vacuum oven for 2 h at 50 °C to produce a 0.17–0.22 mm thick PGSU-CNTs composite film.

2.4. Physicochemical characterization of PGSU-CNTs nanocomposites

The surface morphology of pristine PGSU and PGSU-CNTs films was characterized by SEM (FEI Quanta 3D FEG dual beam scanning electron microscope, 5–10 kV). UV–Vis absorption spectra were measured with a Specord 200 spectrophotometer in the spectral range of 300–900 nm. Samples were prepared into 2.5 mm × 50 mm films, and a Zwick Roell TH1S Z2.5 testing machine with 100 kN load cell was used to determine the elastic modulus, the stress as well as the percentage elongation at the point of failure at a constant strain rate of 20 mm min^{-1}.

To assess the *in vitro* degradation profile of PGSU-CNTs nanocomposites, solvent cast samples (0.6 cm^2) were exposed to physiological conditions (37 °C, PBS, agitation) over a 10-week period. Composite weight was monitored by freeze drying the samples and weighing on an electronic balance on a weekly basis.

2.5. Electrochemical characterization of PGSU-CNTs nanocomposites

Electrochemical impedance spectroscopy (EIS) and cyclic voltammetry (CV) experiments were performed at room temperature (~20 °C) using a Princeton Applied Research Potentiostat/Galvanostat Parstat 2273. The experiments were performed in a 1 ml three-electrode electrochemical cell filled with 0.1 M KCl solution in deionized water (Grade

1, R > 10 MΩ/cm), with pristine PGSU or PGSU-CNTs films as a working electrode, platinum wire as a counter electrode and Ag/AgCl (3.5 M KCl) as a reference electrode. For EIS measurements, a Frequency Response Analyzer was used in a multi-sine mode to cover the range 0.1 Hz–100 kHz. An AC sine wave of 40 mV (*vs.* Ag/AgCl) amplitude was applied with a 0 V DC (*vs.* Ag/AgCl) offset as reported previously [40]. The results were presented as a Bode plot and compared to those of a bare Pt electrode. CV curves were recorded in 0.1 M KCl at a scan rate of 0.1 V/s within a scan window of −0.5 V to 1.5 V (*vs.* Ag/AgCl) for 5 potential cycles. Resulting CV curves were used to determine the charge storage capacity (CSC), calculated as the electric charge integrated under the CV curve during one CV cycle, according to the formula:

$$CSC = \int_{t1}^{t2} I(t)dt$$

where: t_1 is the time at the beginning of a CV cycle (s), t_2 is the time at the end of a CV cycle (s), and I is the current density (A/cm^2).

Integration of CV curves was carried out with Origin 2017 software, as the absolute area of a CV curve. The measurements were performed in triplicate and the results expressed as mean ± standard deviation.

2.6. Fabrication and characterization of PGSU-CNTs nanocomposite strain sensors

To fabricate PGSU-CNTs derived strain sensors, pristine PGSU membranes (47 mm × 30 mm) and 4 wt% CNT PGSU membranes (30 mm × 20 mm) were cut from cast thin films. Interdigitated electrodes were printed onto PGSU-4 wt% CNTs films *via* sputtering a 100 nm layer of gold through a 3D printed mask using an Emitech Sputter Coater (K650XT). The PGSU-4 wt% CNT membrane was subsequently sandwiched between two insulating pristine PGSU membranes. The insulating layers of the sandwich system were coated with glycerol and subsequently heat laminated at 80 °C.

2.7. Cell culture procedure

Primary cultures of ventral mesencephalic (VM) cells were obtained from embryonic Sprague–Dawley rats in accordance with the methods described previously [41] – the detailed procedure is described in Supplementary Information, S1. Pristine PGSU and PGSU-CNT nanocomposite films were cut to fit into 48 well culture plates, sterilized in 70% ethanol, coated with poly-lysine and washed in PBS. 50,000 cells/cm^2 were seeded onto each film and cultured for ten days. Indirect double-immunofluorescent labelling was performed to visualize neuron and astrocyte cell populations as described previously [41,42]. After immunofluorescent staining, samples were viewed with an Olympus Fluoview 1000 Confocal Microscope. For each group, at least 20 random images were taken and analyzed as reported previously [42]. Counting of nuclei corresponding to astrocytes and neurons, respectively, was used to assess cell density. Stereological methods as described previously [43] were used to quantify neurite length using a formula [44]:

$$L = nT\frac{\pi}{2}$$

where: L is the neurite length (μm), n is the number of times neurites intersect applied gridlines, and T is the distance between these gridlines (μm).

All experiments were conducted in biological triplicate. The results were expressed as the mean of the values ± standard error of the mean. Statistical significance ($p < 0.05$) was determined through one-way ANOVA analysis followed by a Bonferroni test.

3. Results and discussion

3.1. Structural characterization of CNTs

The first step in the fabrication of PGSU-CNTs strain sensing devices was to achieve a good dispersion of debundled CNTs in the PGSU elastomer matrix, which allowed for the formulation of an electrically conducting elastomeric nanocomposite. Typically, the entropic gain for the PGSU matrix associated with agglomerated CNTs leads to phase separation of the reinforcement [45]. Therefore, to achieve thermodynamic stability of CNTs dispersed in PGSU, the introduction of additional (repulsive) interactions among the CNTs to overcome entropic and energetic driving forces and suppress aggregation was required [45]. To obtain sufficient dispersion of CNTs in the PGSU matrix, it was necessary to modify the surface of CNTs by a simple non-covalent wrapping process *via* electrostatic deposition. The functionalization technique employed in this study was based on electrostatic self-assembly, a well-established method for the formation of nanocoatings on a broad range of nanoparticles and nanotubes [46]. Here, a strong cationic polyelectrolyte, PAH was used to bind a strongly anionic polyelectrolyte, PEDOT:PSS for the functionalization of CNTs.

It should be noted that PEDOT:PSS functionalization was, employed in this study for two reasons. Firstly, to promote thermodynamic stability of CNTs dispersed in PGSU, allowing homogenous dispersion. Secondly it can be hypothesized that PEDOT:PSS functionalization of CNTs will facilitate ionic transfer at the nanocomposite surface, a critical consideration in neural interface design.

Fig. 1A shows TEM images of pristine CNTs, in which the multiple walls of individual nanotubes are clearly observed. TEM imaging of PAH-CNTs (Fig. 1B), revealed that PAH functionalization invested the tubes completely, acting as a base for the electrostatic assembly of the negatively-charged PEDOT:PSS. The polymer appeared as a 1.5 ± 0.3 nm thick continuous amorphous layer on the nanotubes surface. As seen in Fig. 1C, the PEDOT:PSS layer varied in thickness, ranging from 1.5 nm to 3 nm. Moreover, EDS analysis confirmed this presence of PAH and PEDOT:PSS on the surface of the CNTs during each step of the layer by layer functionalization process (Fig. 1D–E).

The FTIR spectrum of pristine CNTs (Fig. 1F) showed a minor peak at 2970 cm^{-1} ascribed to C–H$_x$ stretching vibrations [47]. However, other peaks at 1738, 1434, 1365 and 1216 cm^{-1} were also observed, corresponding to the C═O stretching of COOH [48–50]. PAH-functionalized CNTs presented a peak at 1646 cm^{-1} (stretching of the N—H bonds of a primary amine), a peak at approximately 1457 cm^{-1} (symmetric deformation vibrations of CH_2-N^+H_3) and a minor peak at 993 cm^{-1} (vibrational modes of R-CH=CH_2) [50]. FTIR spectra of functionalized CNTs showed absorbance peaks at 1510, 1135, 1093, 943 and 860 cm^{-1} corresponding to C═C stretching in the thiophene ring of the ethylenedioxy group, stretching of C-O-C bonds and S═O stretching of SO_3 respectively [51]. Critically, characterization of pristine and functionalized CNTs *via* TEM and FTIR confirmed that both polyelectrolytes remained wrapped *via* strong electrostatic interaction after centrifugation.

According to zeta-potential distribution, pristine CNTs were the most negatively charged of all experimental CNTs formulations. After functionalization with PAH, the surface charge was converted to positive, and after PEDOT:PSS functionalization CNTs reverted to a negatively charged state (Fig. 1G).

In the temperature range studied during TGA analysis (Fig. 1H), pristine CNTs did not undergo any significant weight loss attributed to thermal degradation, whereas functionalized CNTs lost more than 20% of their initial weight in four weight loss events. There was a 6.5% weight loss from 40 to 90 °C due to an initial loss of bound water and solvents inside the complex polymers, and an endothermic peak also appeared at 50 °C. The next three weight loss events, which were clearly displayed as three peaks at 365, 440 and 510 °C in the δTGA profile, can be ascribed to the thermal decomposition of the three polymers (PAH,

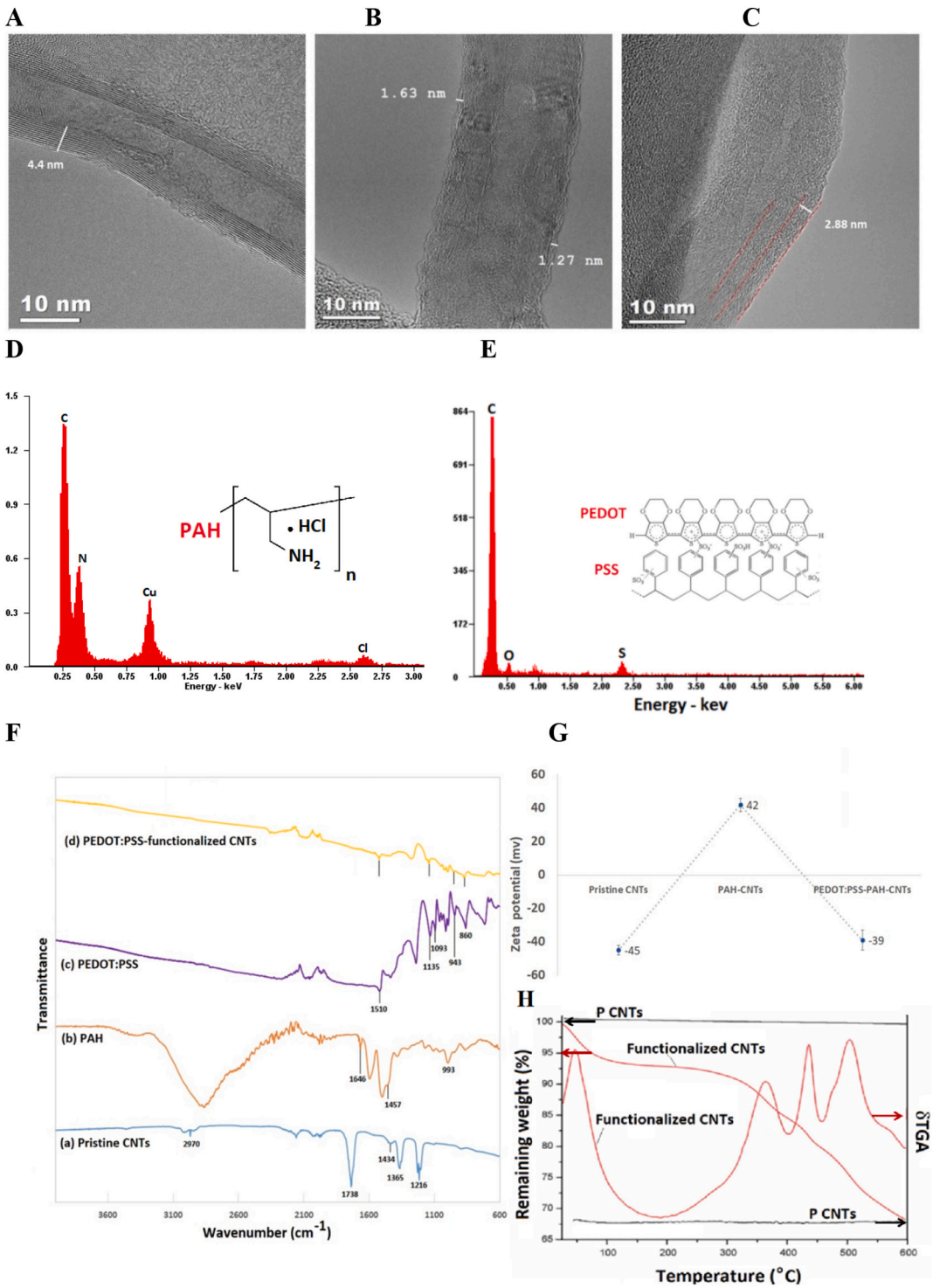

Fig. 1. TEM images of A) pristine CNTs; B) PAH functionalized CNTs; C) PAH/PEDOT:PSS functionalized CNTs; D) EDS spectrum of PAH functionalized nanotubes; E) corresponding EDS spectrum of PAH/PEDOT:PSS functionalized CNTs; F) FTIR spectra; G) zeta potentials; H) TGA and δTGA curves of pristine and functionalized CNTs.

PEDOT and PSS respectively) that coated the surface of the CNTs [52–54]. In this way, it was clearly demonstrated that the surface of CNTs was successfully functionalized with PAH and PEDOT:PSS. Furthermore, the composition ratio between the polyelectrolytes and CNTs was evaluated to be around 25%, proving the formation of a core–shell structure with two investing polymer layers.

3.2. Physicochemical analysis of PGSU-CNTs

Filler interconnectivity in random systems is highly dependent on the polymer chemistry, processing techniques, temperature, size of nanotubes and their electrostatic interactions [55]. Fig. S1A shows SEM micrographs of the top surface of a pristine PGSU film, presenting a rough surface after slow solvent removal and drying. Conversely, a dense sub-structural architecture was identified in the polymer

nanocomposites (Fig. S1B–E). Here, dispersed CNTs in a PGSU matrix presented a non-uniform nanoscale mesh-like structure of entangled CNTs coated in PGSU. The density of these CNT structures increased with CNTs content, producing locally anisotropic but globally isotropic networks with a high degree of interconnectivity and a percolated microporous structure. At lower CNT loadings, the formation of larger pores was evident, which can be hypothesized prevented the formation of a percolated network. Increasing the CNTs weight fraction to 4 wt% resulted in the formation of a physically connected network, necessary to reach the electrical percolation threshold [56].

FTIR analysis was conducted on both pristine PGSU and PGSU-CNT nanocomposites formulated with 4% and 5% CNTs to confirm the formation of polyurethane and to monitor the interactions between PGSU and CNTs (Fig. S2A). Pristine PGSU spectra demonstrated a band at 3325 cm^{-1} (stretching of O—H and N—H) and further bands at 2930 and 2854 cm^{-1} (asymmetric and symmetric stretching of -CH_2) [57]. A peak at ~1700 cm^{-1} was assigned to the stretching of the C═O bond from ester and amide groups, and peaks at 1618 and 1535 cm^{-1} were attributed to the amide I and amide II groups of urethane, the reaction product of the crosslinking agent and hydroxyl groups [36]. These results verified the crosslinking process of the PGS pre-polymer with HDI and PGSU synthesis as observed previously [28,29].

Conversely, the appearance of a minor peak at 860 cm^{-1} in both 4% and 5% CNTs nanocomposites was attributable to the C—S vibration band in the thiophene rings of PEDOT, confirming the presence of functionalized CNTs in PGSU matrix.

By increasing the content of wrapped CNTs to 2 wt%, absorbance curves (Fig. S2B) showed strong absorption in the UV region. However, the curves of 4 and 5 wt% CNTs nanocomposites illustrated a minor transmission from the UV to the NIR region.

3.3. Electrochemical analysis of PGSU-CNTs

Pristine PGSU and PGSU-CNTs nanocomposites containing less than 2 wt% of CNTs, demonstrated a noisy and high impedance profile (Fig. 2A), indicating that these materials can be considered as insulators rather than semiconductors or conductors. With increasing CNT content, however, the electrochemical impedance was significantly reduced, achieving a percolation threshold for PGSU nanocomposites with 4 wt% CNT content. At the reference frequency of 1 kHz, which is relevant to neuronal signal recording and used to compare the impedance among electrode materials [58–61], the impedance of 4 wt% CNTs (2.6 ± 0.4 kΩ) and 5 wt% CNTs (1.6 ± 0.4 kΩ) was significantly lower that the impedance of PGSU-2 wt% CNTs (2.3 ± 1.8 MΩ) and pristine PGSU (11.0 ± 3.8 MΩ).

PGSU-CNT nanocomposites were also shown to possess a low impedance profile at higher frequencies, relevant for high-frequency neural stimulation [62], which was observed to reach a minimum for PGSU-5 wt% CNTs at 10 kHz (204 ± 44 Ω) (Fig. 2B). The phase angle *vs.* frequency Bode plots (Fig. S3) for PGSU-4 wt% CNTs and PGSU-5 wt% CNTs indicated the capacitive behavior of these nanocomposites, and a well-defined capacitive peak was present at the frequency of ~1 kHz, significantly higher than for Pt control electrodes (~1 Hz). Due to the low conductivity, however, the phase angle *vs.* frequency plots for PGSU-CNTs nanocomposites with CNT loading ≤ 2 wt% were noisy, making them difficult to analyze.

The onset of the Maxwell-Wanger-Sillars (MWS) relaxation frequency was observed at ~1 kHz (Fig. S4). At this frequency, the nanocomposites demonstrated resistive behavior, sensitive to deformation due to relative phase changes as well as piezoresistive changes upon deformation. Hence, a frequency of 1 kHz was subsequently used to analyze the piezoresistive behavior of this nanocomposite in the strain sensor study described below.

Cyclic voltammetry (Fig. 2C) confirmed a significant increase in the nanocomposite CSC with increasing CNTs content (1508.22 ± 3.92 μC cm^{-2} for PGSU 5 wt% CNTs) relative to pristine PGSU formulations

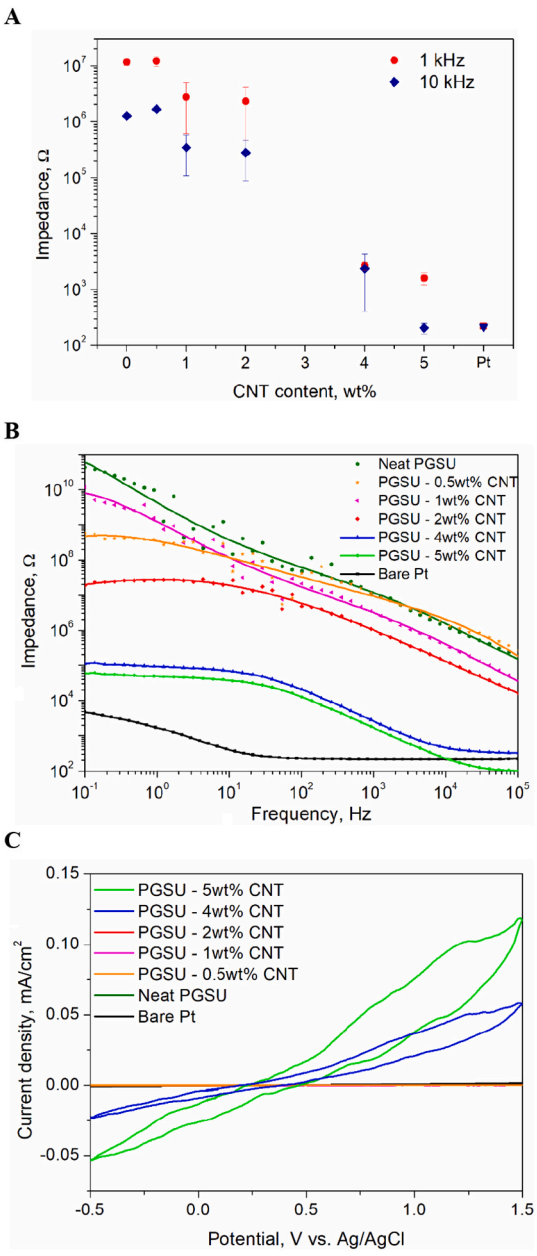

Fig. 2. The influence of PEDOT:PSS functionalized CNT content on the electrochemical properties of PGSU nanocomposite electrodes. A) The impedance modulus as a function of frequency; dots represent the experimental points and lines represent modelled data. B) The impedance of nanocomposite electrodes at 1 kHz and 10 kHz was significantly reduced relative to control pristine PGSU samples. C) Representative CVs of pristine PGSU, PGSU-CNT nanocomposites and a control Pt electrode.

(0.22 ± 0.01 μC cm^{-2}). In particular, PGSU-CNTs nanocomposites with 4 wt% and 5 wt% CNT contents were observed to outperform a platinum electrode, which possessed a CSC of 25.33 ± 0.28 μC cm^{-2} (Table S1), reaching a 60-fold and 30-fold increase in CSC (for PGSU-5 wt% CNT and PGSU-4 wt% CNT, respectively).

Electrochemical impedance data confirmed that the electrical properties of PGSU-CNTs nanocomposites were strongly dependent on the weight fraction of CNTs reinforcement, and the percolation threshold was determined by a decrease in the electrical resistance. A three order of magnitude decrease in electrical impedance was also observed between PGSU samples loaded with 2 wt% and 4 wt% CNTs, where the impedance at 1 kHz changed from 2.3 ± 1.8 MΩ to ~2.6 ± 0.4 kΩ,

Although the percolation threshold appeared to lie higher than that of other polymer-CNTs composites (typically reported between 0.5 and 3.2 wt% CNTs) [63–65], the nanocomposites investigated in this study were found to possess a low impedance profile at high frequencies (10 kHz).

3.4. Mechanical properties of PGSU-CNTs

Tensile properties of composite films with six weight fractions (0, 0.5, 1, 2, 4 and 5%) of functionalized CNTs were examined. Typical stress-strain curves (Fig. 3A) and mean elastic modulus (Fig. 3B) were obtained for pristine PGSU (Video S1) and PGSU-CNT nanocomposites. For each weight fraction, three specimens were considered, and the mean values of the mechanical properties were recorded. The initial linear slope of the stress-strain curves represented the elastic modulus whereas tensile strength and strain at break were obtained from the point of sample failure [66]. The presence of PEDOT:PSS functionalized CNTs increased the elastic modulus of PGSU to 36.63 MPa *via* incorporation of 5 wt% CNT reinforcement.

A similar trend was observed for the ultimate tensile strength, which increased as a function of CNT content. Conversely, the strain at break of nanocomposites decreased with increasing CNT content for all PGSU-CNT nanocomposites (Fig. 3C). As shown in Fig. 3D, a 60% improvement in the toughness of PGSU formulations (given by the area under the stress – strain curve [67]) resulted from the formation of a percolated network of uniformly dispersed functionalized CNTs into the PGSU matrix [36].

From a mechanical point of view, the dual layer PAH-PEDOT:PSS assembly explored in this study promoted a stable interface between the CNTs and the PGSU matrix, facilitating the transfer of mechanical loads from the matrix to the reinforcement *via* shear stress [68,69]. The tensile test results confirmed that the incorporation of functionalized CNTs into PGSU significantly modulated the mechanical properties of all studied nanocomposites. It is noteworthy that the promising interfacial adhesion of functionalized CNTs within the PGSU matrix provided an apparent improvement in tensile modulus and toughness as a function of CNT content.

3.5. Stress/strain sensing of PGSU-CNTs

Pathological tissue stress in particular mechanical stresses associated with brain swelling [70,71], have been reported in the 1–100 kPa range. Therefore, in order to examine the performance of neural-specific PGSU-CNTs strain sensor, we applied a cyclic strain of 1% at a frequency of 0.5 Hz for 62 h, corresponding to a stress in the order of tens of kPa (Fig. 3A).

As PGSU-CNTs nanocomposites formulated with 4 wt% and 5 wt% CNT content possessed similar electrochemical properties, only the PGSU 4 wt% CNT formulation was brought forward for incorporation into a strain sensing device (Fig. 4A). At the percolation threshold, this material demonstrated relatively low impedance at 1 kHz, which was identified as being near the MWS relaxation frequency, ensuring that the nanocomposites were sensitive to changes in strain, resulting from dynamic electrical continuity and discontinuity within the conductive network. Fig. 4B demonstrates the relative change in impedance as a function of time in PGSU-CNTs strain sensors undergoing 0.5 Hz cyclic loading and measured at a frequency of 1 kHz. The relative impedance measured before cyclic loading remained constant, increasing upon stress loading and decreasing upon stress unloading. The relative change in impedance was 32 ± 12% during the initial loading regimen at day 1 and was reduced over time as suggested by the strain gauge factor (Fig. 4C). Sensors were under continuous cyclic loading and unloading conditions over a period of four days and underwent 43,200 cycles over a period of 24 h. Due to a continuous hysteresis loss, associated with the viscoelastic behavior of pristine PGSU and PGSU nanocomposites during the cyclic loading conditions, a change in piezoresistive behavior of the sensor was observed, in agreement with Mullin's damage model [72]. The strain magnitude and the number of strain cycles caused a sufficient change in the bonding of CNTs to the PGSU matrix, subsequently reducing the gauge factor with time. It is suggested that this reduction could be mitigated through further optimization of processing conditions as described previously [72].

The device strain gauge factor was calculated using GF = ΔZ / (Z0 * ε), where ΔZ = change in impedance (impedance at initial time point, without mechanical loading / average impedance measured during cyclic loading for other time points (Z0)). The impedance measured at 1%

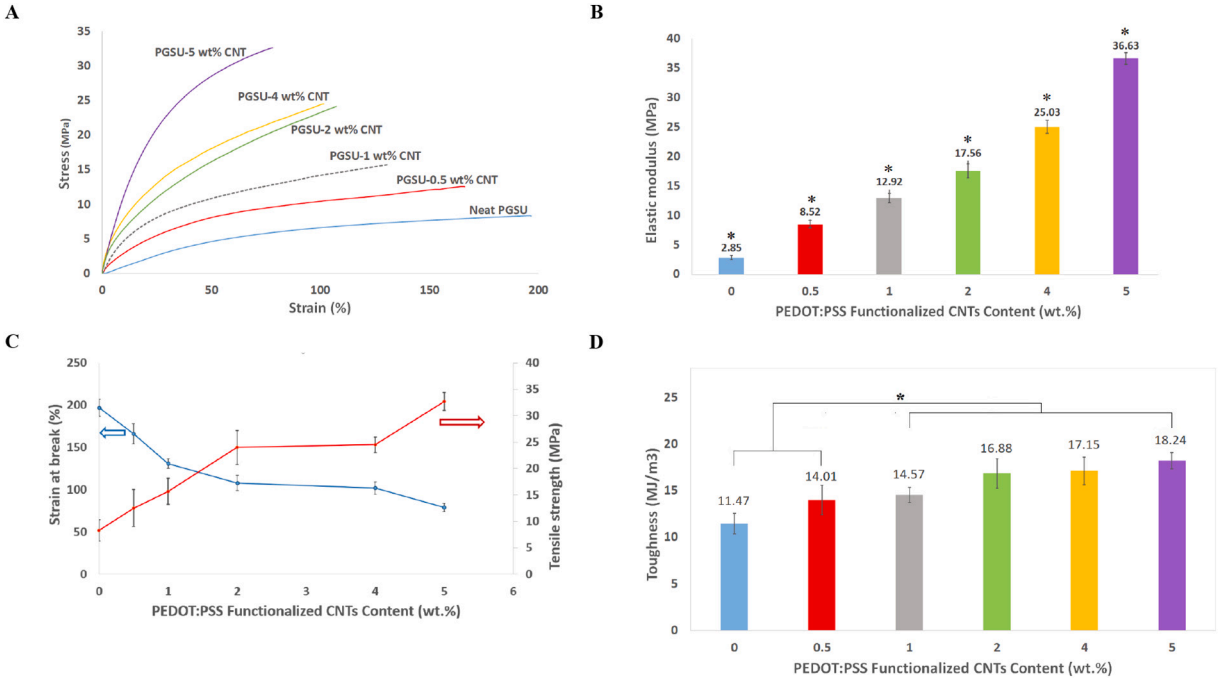

Fig. 3. Mechanical analysis of pristine PGSU and PGSU-CNT nanocomposites. A) Representative tensile stress-strain curves; B) mean elastic modulus; C) elongation at break and tensile strength; D) mean toughness as obtained from area under the stress–strain curve (extracted from A). Bar graphs are ±STD, $p < 0.05$.

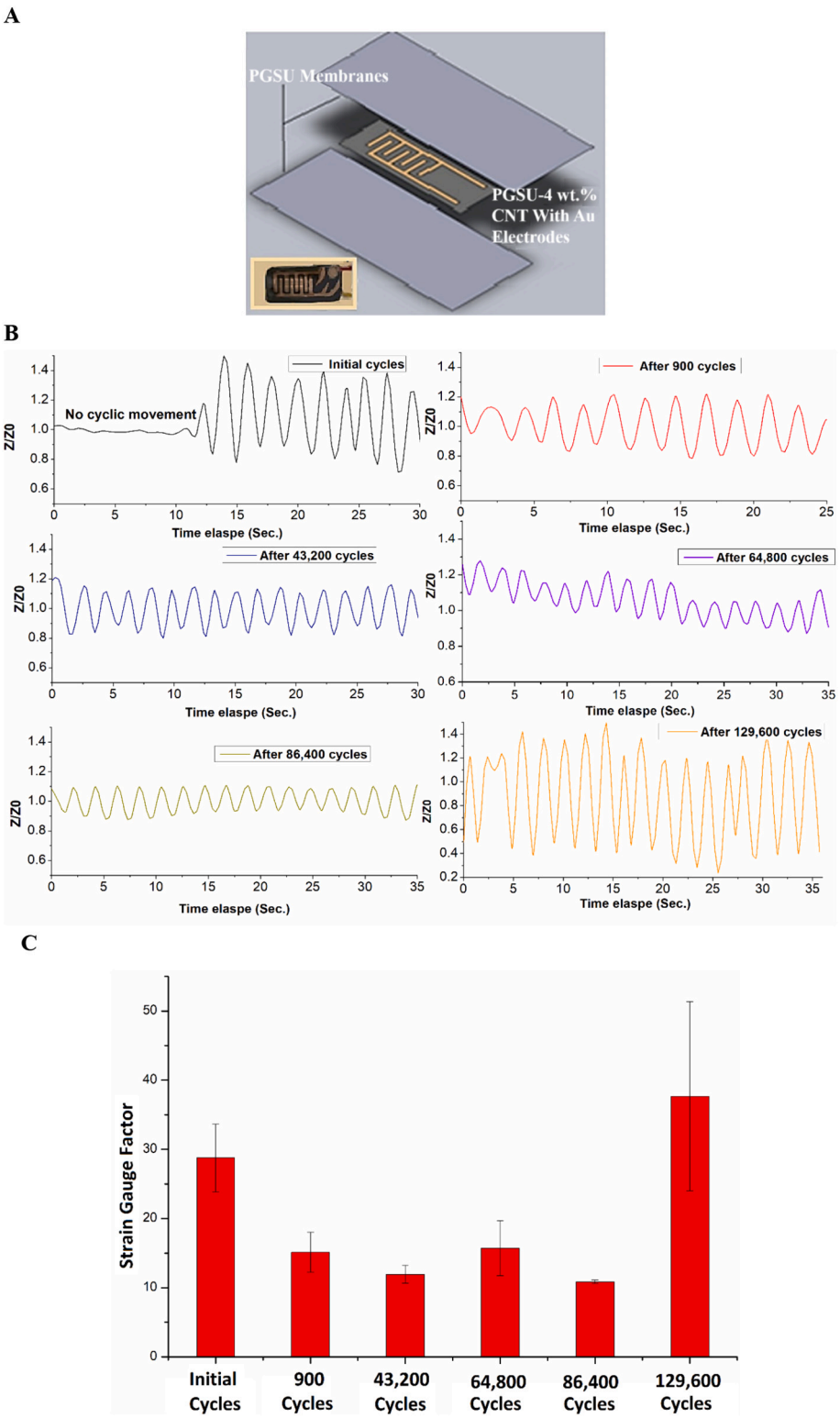

Fig. 4. A) Schematic of the stress/strain sensor fabricated from pristine and composite PGSU-4 wt% CNT films. Gold interdigitated electrodes were deposited onto a PGSU-4 wt% CNTs membrane which was laminated between two pristine PGSU membranes; B) relative change in impedance over 130,000 cycles of 1% strain at 0.5 Hz; C) the strain gauge factor over 1 of 1% cyclic strain at 0.5 Hz.

strain (ε) was observed to range from 25 to 35 (for initial cycles) and to stabilize between 11 and 16 after 43,200 cycles for all sensors measured. This response was highly repeatable (n = 3). Here, changes in the resistive behavior of the sensors were more prominent than changes in capacitive behavior as the sensor measurements were taken at the onset of the MWS relaxation frequency (Fig. S5).

An inherent property of elastomers is the direct relationship between strain and electrical resistance, arising from molecular alignment [73]. In this work, due to the uniform dispersion of the conducting particles in the PGSU matrix, uniform changes in electrical impedance were

observed on the application of cyclic strain. During the initial 1% strain cycles these changes were significantly higher than changes obtained after 900 strain cycles. This effect can be directly compared with strain/strain relaxation phenomena or loss energy as described previously [19,74]. After 900 cycles under simulated physiological conditions, strain induced changes in electrical impedance became stable and the strain gauge factor remained within a narrow range. This strain gauge stabilization can be attributed to a dynamic equilibrium in bond breakage and bond formation between CNTs and the PGSU polymer matrix during mechanical loading and unloading conditions. After 86,400 strain cycles, the impedance of the sensor was found to decrease from the MΩ to kΩ range before the sensor started to fail due to delamination of the PGSU insulation, resulting in an influx and outflux of PBS into the sensor. It can be reasoned that delamination of the sensors could be negated by laminating the active layer of the sensor through a dip coating process in a highly viscous PGS pre-polymer formulation prior to crosslinking.

3.6. Biological characterization of PGSU-CNTs

Preliminary assessment of the biocompatibility of PGSU-CNT nanocomposites was provided through a LIVE/DEAD® assay with human tenocytes cultured for 1, 7 and 14 days on pristine PGSU and PGSU-CNTs nanocomposites, as well as a glass control substrate (Fig. S6). The percentage of live cells found on the surface of PGSU-CNTs nanocomposites was higher or equal to the percentage of live cells found on a control substrate (glass), and always exceeded 97% viability. Interestingly no dead cells were found on the surface of any of the investigated PGSU-CNTs composites after 14 days of cell culture, indicating biocompatibility, as described in ISO 10993-5 [75].

Fig. 5A–D shows representative fluorescent micrographs of mixed population VM cells (neurons and astrocyte) cultured on pristine PGSU and PGSU-CNTs nanocomposites over a period of ten days. Analysis of the percentage of astrocytes and neurons present indicated no statistical differences between groups (Fig. 5E). Here all experimental and control groups were associated with the presence of approx. 50% astrocyte and 50% neural cell presence by day 10. This is consistent with previous studies which have shown that CNTs and PEDOT-CNT formulations are non-cytotoxic and can be employed to promote mature synapse formation and tune the neuronal network architecture [76–78].

Significant differences were observed in the neurite outgrowth of VM neurons, however (Fig. 5F). The neural length was observed to significantly decrease from 112 ± 2.3 mm on pristine PGSU to 66.3 ± 1.4 mm on PGSU 1 wt% CNTs, and further decreased on PGSU 4 wt% CNTs, which possessed an average neurite length of 33 ± 1.5 mm. This observation is consistent with previous studies, in which CNTs are found to perturb the growth and branching of neurons [79] *in vitro*. This effect may be addressed in future studies however, by further functionalization of the CNTs, to control the outgrowth of neuronal processes [80] and to promote CNT biodegradation [81,82].

3.7. In vitro degradation behavior of PGSU-CNTs

Observed reductions in the mass of PGSU and PGSU-CNTs nanocomposites maintained at 37 °C in PBS (Fig. S7A) indicated that all investigated materials underwent hydrolytic degradation. A mean 11%

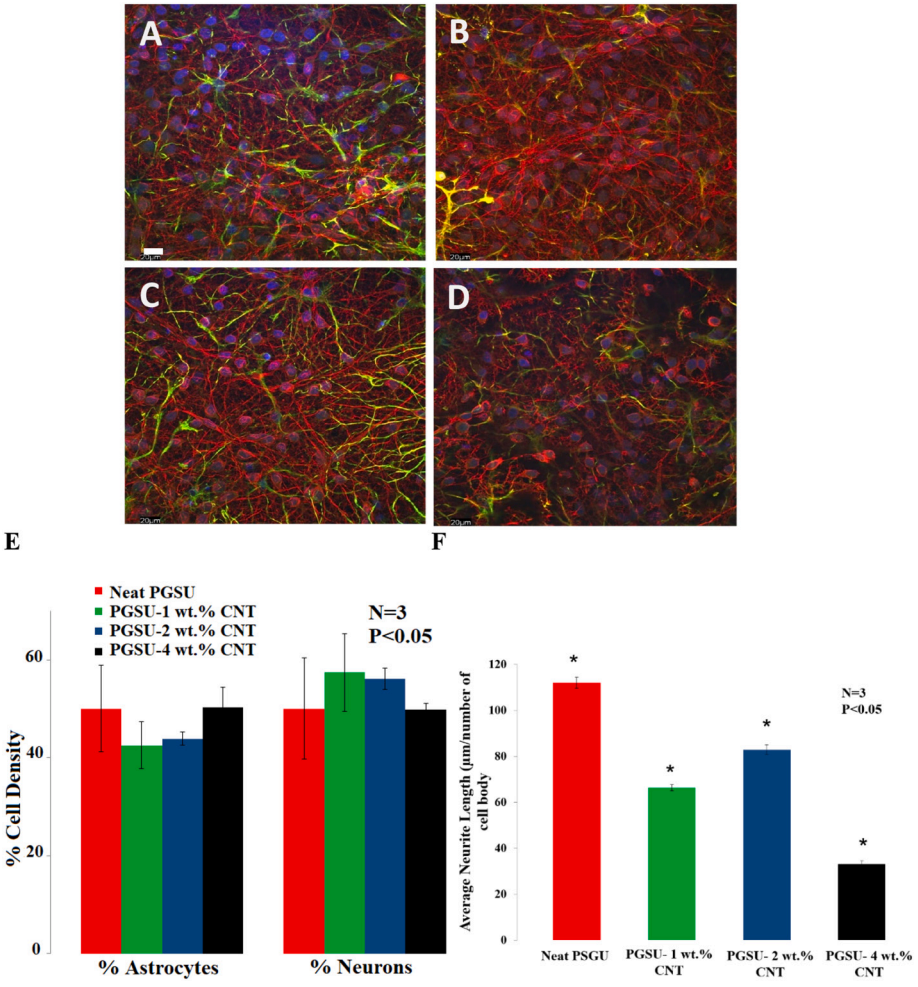

Fig. 5. Representative fluorescent images of primary VM mixed cell population grown on PGSU and CNT nanocomposite formulations for ten days; A–D) PGSU - 0, 1, 2 and 4 wt% CNTs respectively. Neurons were visualized by anti β-tubulin III, in red, astrocyte cells by anti-GFAP, in green, and nuclei by DAPI, in blue. Bar = 20 μm. Results are ±STD. Cytocompatibility analysis of VM cells cultured on pristine and PGSU-CNTs nanocomposite formulations for 10 days. E) Cell density (%) analysis of astrocytes and neurons; F) neural length analysis. (For interpretation of the references to color in this figure legend, the reader is referred to the web version of this article.)

mass loss was noted for pristine PGSU after 10 weeks. Conversely, PGSU 0.5 wt% CNT composites demonstrated the fastest degradation rate (16% by 10 weeks). The highest stability was noted for PGSU 4 wt% CNTs and PGSU 5 wt% CNTs, for which the mean mass loss after 10 weeks was 8%. Spectrophotometric assessment of the PBS supernatant confirmed that CNTs did not leach from PGSU-CNTs nanocomposites during hydrolytic degradation (Fig. S7B).

FTIR spectra of PGSU 4 wt% CNT nanocomposites obtained before and after the degradation study (Fig. S8A) demonstrated absences in the signals assigned to stretching of O—H and N—H (3325 cm^{-1}), as well as a decrease in signal intensities at 2930 cm^{-1} and 2854 cm^{-1} (asymmetric and symmetric -CH_2 stretching respectively, characteristic for PGSU). Concurrently, an increase in the intensity of peaks at 2960 cm^{-1} and 1726 cm^{-1} (CNTs associated OH stretching and C═O stretching, respectively) was observed. SEM images of degraded PGSU-CNTs nanocomposites confirmed that although CNTs became exposed after being subjected to hydrolysis, the presence of a signal at 1092 cm^{-1} indicated that CNTs were still coated with PEDOT:PSS after this process (Fig. S8B).

The exposure of CNTs because of the degradation of PGSU had a positive effect on the electrochemical performance of the composite materials. Fig. S8C shows that the CV of PGSU 4 wt% CNTs nanocomposite subjected to degradation was expanded when compared to a non-degraded material. Through the degradation of PGSU matrix, the CSC increased by 68%, from 1508 $\pm$ 4 μC cm^{-2} to 2540 $\pm$ 57 μC cm^{-2}. Similarly, the electrochemical impedance profile was observed to decrease at frequencies below 3 kHz relative to non-degraded composites (Fig. S8D).

Finally, the PGSU matrix of the composite materials was observed to undergo stable hydrolysis *in vitro*, loosing approx. 1% of its mass every week. Although the change in mass of the nanocomposites examined in this study was attributed exclusively to the hydrolytic degradation of PGSU, previous studies have indicated that carbon-based nanostructures, including CNTs, are able to undergo degradation *in vitro* and *in vivo* through the action of macrophages [81,82]. Furthermore, it is envisaged that the polymers could be optimized for specific degradation rates by altering chain length and/or the stereochemistry of the PGSU.

The PGSU-CNTs sensor developed in this study was designed to partially degrade after its useful lifetime, which for a pressure sensor usually lies between 290 and 400 days [83]. Although it can be suggested that the CNT and PEDOT elements of the device will undergo limited degradation *in vivo* [84], future studies employing fully degradable filler elements (*i.e.* Mg nanowires) may lead to the realization of fully degradable strain sensor devices. Critically, by designing a strain sensor made exclusively of biodegradable materials the need for surgical extraction would be avoided [85,86] and controlled degradation kinetics would allow monitoring of mechanical deformations and pressures in real time *in vivo*, achieving a refined and personalized medical approach, resulting in total device degradation [86,87].

4. Conclusions

Here, PAH-PEDOT:PSS functionalized CNTs were incorporated into a PGSU matrix during the polymerization process, to produce a biodegradable and electrically conductive elastomer. The presence of a functionalized CNT network improved the electrical and mechanical properties of the polymer while maintaining the materials biodegradability and cytocompatibility. The PGSU 4 wt% CNTs nanocomposite was found to possess a high charge storage capacity (1508 $\pm$ 4 μC cm^{-2}) and a low electrochemical impedance at 10 kHz (204 $\pm$ 44 Ω), outperforming a pristine platinum electrode. Critically, PGSU 4 wt% CNT nanocomposites showed optimal sensitivity to applied 1% uniaxial tensile strain and could be formulated into a flexible and durable pressure sensor. Cytocompatibility analysis with a mixed neural population showed that both pristine PGSU and conductive PGSU-CNTs nanocomposites could support cell adhesion and survival after long-term culture. These results demonstrated that PGSU-CNTs nanocomposites were elastic, conducting, and biocompatible materials suitable for soft tissue engineering and bioelectronic applications.

Supplementary data to this article can be found online at https://doi.org/10.1016/j.msec.2020.111857.

Declaration of competing interest

The authors declare that they have no known competing financial interests or personal relationships that could have appeared to influence the work reported in this paper.

Acknowledgements

This publication has emanated from research conducted with the financial support of the Science Foundation Ireland (SFI) Technology Innovation Development Programme, grant no. 15/TIDA/2992 and was co-funded under the European Regional Development Fund under Grant Number 13/RC/2073. The authors acknowledge the facilities and scientific and technical assistance of the Centre for Microscopy & Imaging at the National University of Ireland Galway, a facility that is funded by NUIG and the Irish Government's Programme for Research in Third Level Institutions, Cycles 4 and 5, National Development Plan 2007–2013.

References

[1] H. Shi, H. Liu, S. Luan, D. Shi, S. Yan, C. Liu, R.K.Y. Li, J. Yin, Compos. Sci. Technol. 127 (2016) 28–35.
[2] X. Zhang, X. Peng, S.W. Zhang, 1 - Biodegradable Medical Polymers: Fundamental Sciences, Woodhead Publishing, Science and Principles of Biodegradable and Bioresorbable Medical Polymers, 2017, pp. 1–33.
[3] A.J. Hackett, J. Malmström, J. Travas-Sejdic, Prog. Polym. Sci. 70 (2017) 18–33.
[4] L. Poole-Warren, N. Lovell, S. Baek, R. Green, Exp. Rev. Med. Devices 7 (2010) 35–49.
[5] R.A. Green, N.H. Lovell, G.G. Wallace, L.A. Poole-Warren, Biomaterials 29 (2008) 3393–3399.
[6] V. Sencadas, C. Tawk, G. Alici, ACS Appl. Mater. Interfaces 12 (2020) 8761–8772.
[7] M. Irimia-Vladu, E.D. Głowacki, G. Voss, S. Bauer, N.S. Sariciftci, Mater. Today 15 (2012) 340–346.
[8] M. Humar, S.J. Kwok, M. Choi, A.K. Yetisen, S. Cho, S.-H. Yun, Nanophotonics 6 (2017) 414–434.
[9] R.K. Pal, A.A. Farghaly, C. Wang, M.M. Collinson, S.C. Kundu, V.K. Yadavalli, Biosens. Bioelectron. 81 (2016) 294–302.
[10] A.C. Patil, Z. Xiong, N.V. Thakor, Small Methods 4 (2020) 2000274.
[11] A.B. Kaiser, V. Skakalova, Chem. Soc. Rev. 40 (2011) 3786–3801.
[12] M.D. Angione, R. Pilolli, S. Cotrone, M. Magliulo, A. Mallardi, G. Palazzo, L. Sabbatini, D. Fine, A. Dodabalapur, N. Cioffi, L. Torsi, Mater. Today 14 (2011) 424–433.
[13] H. Zhou, G. Han, Electrochim. Acta 192 (2016) 448–455.
[14] A. Rabti, N. Raouafi, A. Merkoçi, Carbon 108 (2016) 481–514.
[15] J. Guo, Y. Liu, R. Prada-Silvy, Y. Tan, S. Azad, B. Krause, P. Pötschke, B.P. Grady, J. Polym. Sci. B Polym. Phys. 52 (2014) 73–83.
[16] C. Ding, K. Liu, C. Guo, D. Jia, B. Cheng, Polym. Eng. Sci. 56 (2016) 408–417.
[17] B. Li, J. Luo, X. Huang, L. Lin, L. Wang, M. Hu, L. Tang, H. Xue, J. Gao, Y.-W. Mai, Compos. Part B 181 (2020) 107580.
[18] J. Hwang, J. Jang, K. Hong, K.N. Kim, J.H. Han, K. Shin, C.E. Park, Carbon 49 (2011) 106–110.
[19] A. Poudel, N. Karode, P. McGorry, P. Walsh, J.G. Lyons, J. Kennedy, S. Matthews, A. Coffey, Compos. Part B 165 (2019) 397–405.
[20] J. Narongthong, H.H. Le, A. Das, C. Sirisinha, S. Wießner, Compos. Sci. Technol. 174 (2019) 202–211.
[21] G. Kaur, R. Adhikari, P. Cass, M. Bown, P. Gunatillake, RSC Adv. 5 (2015) 37553–37567.
[22] H.-J. Kim, K. Sim, A. Thukral, C. Yu, Sci. Adv. 3 (2017), e1701114.
[23] I. Kang, M.J. Schulz, J.H. Kim, V. Shanov, D. Shi, Smart Mater. Struct. 15 (2006) 737–748.
[24] T. Wang, Y. Zhang, Q. Liu, W. Cheng, X. Wang, L. Pan, B. Xu, H. Xu, Adv. Funct. Mater. 28 (2018) 1705551.
[25] J.A. Rogers, T. Someya, Y. Huang, Science 327 (2010) 1603–1607.
[26] Y. Wang, G.A. Ameer, B.J. Sheppard, R. Langer, Nat. Biotechnol. 20 (2002) 602–606.
[27] C. Fidkowski, M.R. Kaazempur-Mofrad, J. Borenstein, J.P. Vacanti, R. Langer, Y. Wang, Tissue Eng. 11 (2005) 302–309.
[28] C.A. Sundback, J.Y. Shyu, Y. Wang, W.C. Faquin, R.S. Langer, J.P. Vacanti, T. A. Hadlock, Biomaterials 26 (2005) 5454–5464.

[29] M. Radisic, H. Park, T.P. Martens, J.E. Salazar-Lazaro, W. Geng, Y. Wang, R. Langer, L.E. Freed, G. Vunjak-Novakovic, J. Biomed. Mater. Res. A 86 (2008) 713–724.
[30] Y. Liu, K. Tian, J. Hao, T. Yang, X. Geng, W. Zhang, J. Mater. Sci. Mater. Med. 30 (2019) 53.
[31] L. Jiang, Y. Jiang, J. Stiadle, X. Wang, L. Wang, Q. Li, C. Shen, S.L. Thibeault, L.-S. Turng, Mater. Sci. Eng. C 94 (2019) 740–749.
[32] R. Rai, M. Tallawi, N. Barbani, C. Frati, D. Madeddu, S. Cavalli, G. Graiani, F. Quaini, J.A. Roether, D.W. Schubert, E. Rosellini, A.R. Boccaccini, Mater. Sci. Eng. C 33 (2013) 3677–3687.
[33] Y. Li, W.D. Cook, C. Moorhoff, W.-C. Huang, Q.-Z. Chen, Polym. Int. 62 (2013) 534–547.
[34] G.C. Engelmayr, M. Cheng, C.J. Bettinger, J.T. Borenstein, R. Langer, L.E. Freed, Nat. Mater. 7 (2008) 1003–1010.
[35] R. Ravichandran, J.R. Venugopal, S. Sundarrajan, S. Mukherjee, S. Ramakrishna, Tissue Eng. A 17 (2011) 1363–1373.
[36] T. Wu, M. Frydrych, K. O'Kelly, B. Chen, Biomacromolecules 15 (2014) 2663–2671.
[37] A. Samourides, L. Browning, V. Hearnden, B. Chen, Mater. Sci. Eng. C 108 (2020) 110384.
[38] M. Frydrych, B. Chen, Polymer 122 (2017) 159–168.
[39] M.J. Pereira, B. Ouyang, C.A. Sundback, N. Lang, I. Friehs, S. Mureli, I. Pomerantseva, J. McFadden, M.C. Mochel, O. Mwizerwa, P. Del Nido, D. Sarkar, P.T. Masiakos, R. Langer, L.S. Ferreira, J.M. Karp, Adv. Mater. 25 (2013) 1209–1215.
[40] X.F. Wei, W.M. Grill, J. Neural Eng. 6 (2009), 046008.
[41] C. Vallejo-Giraldo, N.P. Pampaloni, A.R. Pallipurath, P. Mokarian-Tabari, J. O'Connell, J.D. Holmes, A. Trotier, K. Krukiewicz, G. Orpella-Aceret, E. Pugliese, L. Ballerini, M. Kilcoyne, E. Dowd, L.R. Quinlan, A. Pandit, P. Kavanagh, M.J. P. Biggs, Adv. Funct. Mater. 28 (2018) 1–18.
[42] C. Vallejo-Giraldo, E. Pugliese, A. Larranaga, M.A. Fernandez-Yague, J.J. Britton, A. Trotier, G. Tadayyon, A. Kelly, I. Rago, J.R. Sarasua, E. Dowd, L.R. Quinlan, A. Pandit, M.J. Biggs, Nanomedicine (London, England), 11 (2016) 2547–2563.
[43] G.W. O'Keeffe, P. Dockery, A.M. Sullivan, J. Neurocytol. 33 (2004) 479–488.
[44] E.T. Kavanagh, J.P. Loughlin, K.R. Herbert, P. Dockery, A. Samall, K.M. Doyle, A. M. Gorman, Biochem. Biophys. Res. Commun. 351 (2006) 890–895.
[45] G.D. Smith, D. Bedrov, Langmuir 25 (2009) 11239–11243.
[46] M. Keeney, X.Y. Jiang, M. Yamane, M. Lee, S. Goodman, F. Yang, J. Mater. Chem. B 3 (2015) 8757–8770.
[47] V. Ţucureanu, A. Matei, A.M. Avram, Crit. Rev. Anal. Chem. 46 (2016) 502–520.
[48] J.P. Hussain S., Chouksey A. , Raman R., Islam S. , Islam T. and Choudhary P., Journal of Modern Physics, 2(6) (2011) 538–543.
[49] M.M.E.S. Alkhatib M.F., Qudsieh I.Y. and Husain I.A.F. , Journal of Applied Sciences 10 (2010) 2705–2708.
[50] L. Rotariu, O.-M. Istrate, C. Bala, Sensors Actuators B Chem. 191 (2014) 491–497.
[51] S. Rattan, P. Singhal, A.L. Verma, Polym. Eng. Sci. 53 (2013) 2045–2052.
[52] L. Shao, J.L. Lutkenhaus, Soft Matter 6 (2010) 3363–3369.
[53] A.V. Murugan, C.-W. Kwon, G. Campet, B.B. Kale, T. Maddanimath, K. Vijayamohanan, J. Power Sources 105 (2002) 1–5.
[54] I. Ahmad, M. Hussain, K.-S. Seo, Y.-H. Choa, J. Appl. Polym. Sci. 116 (2010) 314–319.
[55] A. Belashi, Percolation Modeling in Polymer Nanocomposites, University of Toledo, 2011.
[56] A.V. Kyrylyuk, P. van der Schoot, Proc. Natl. Acad. Sci. 105 (2008) 8221–8226.
[57] T. Elzein, M. Nasser-Eddine, C. Delaite, S. Bistac, P. Dumas, J. Colloid Interface Sci. 273 (2004) 381–387.
[58] K. Wang, R.Y. Tang, X.B. Zhao, J.J. Li, Y.R. Lang, X.X. Jiang, H.J. Sun, Q.X. Lin, C. Y. Wang, Nanoscale 7 (2015) 18677–18685.
[59] Y. Lu, T. Li, X. Zhao, M. Li, Y. Cao, H. Yang, Y.Y. Duan, Biomaterials 31 (2010) 5169–5181.
[60] M. Kindlundh, P. Norlin, U.G. Hofmann, Sensors Actuators B Chem. 102 (2004) 51–58.
[61] E. Seker, Y. Berdichevsky, M.R. Begley, M.L. Reed, K.J. Staley, M.L. Yarmush, Nanotechnology 21 (2010) 125504.
[62] Y. Jamali, M. Jamali, M. Golshani, arXiv preprint arXiv:1904.12456, (2019).
[63] M.Y.W. Lu C., Journal of Materials Science 43 (2008) 6012–6015.
[64] D.L. Gao, M.S. Zhan, Polym. Compos. 31 (2010) 1084–1090.
[65] X. Zeng, X. Xu, P.M. Shenai, E. Kovalev, C. Baudot, N. Mathews, Y. Zhao, J. Phys. Chem. C 115 (2011) 21685–21690.
[66] J.M. Gosline, P.A. Guerette, C.S. Ortlepp, K.N. Savage, J. Exp. Biol. 202 (1999) 3295–3303.
[67] D. Taylor, J. Mech. Behav. Biomed. Mater. 77 (2018) 776–782.
[68] P. Lv, Y.-y. Feng, P. Zhang, H.-m. Chen, N. Zhao, W. Feng, Carbon 49 (2011) 4665–4673.
[69] J. Biagiotti, S. Fiori, L. Torre, M.A. López-Manchado, J.M. Kenny, Polym. Compos. 25 (2004) 26–36.
[70] U. Kawoos, M. Gu, J. Lankasky, R.M. McCarron, M. Chavko, PLoS One 11 (2016), e0167510.
[71] S. Angeli, T. Stylianopoulos, J. Biomech. 56 (2017) 42–47.
[72] L. Mullins, Rubber Chem. Technol. 22 (1949) 1036–1044.
[73] M.S. Irfan, Y.Q. Gill, S. Ullah, M.T. Naeem, F. Saeed, M. Hashmi, Smart Mater. Struct. 28 (2019), 095024.
[74] A. Poudel, P. Walsh, J. Kennedy, K. Thomas, J.G. Lyons, A. Coffey, J. Thermoplast. Compos. Mater. 32 (2019) 178–204.
[75] S. Ullah, A. Ullah, J. Lee, Y. Jeong, M. Hashmi, C. Zhu, K.I. Joo, H.J. Cha, I.S. Kim, ACS Appl. Nano Mater. 3 (2020) 7231–7241.
[76] B. Dinesh, M. Medelin, D. Scaini, F. Lareno Faccini, F. Quici, L. Ballerini, A. Bianco, ACS Chem. Neurosci. 11 (2020) 162–172.
[77] N.P. Pampaloni, D. Scaini, F. Perissinotto, S. Bosi, M. Prato, L. Ballerini, Nanomed. Nanotechnol. Biol. Med. 14 (2018) 2521–2532.
[78] X. Luo, C.L. Weaver, D.D. Zhou, R. Greenberg, X.T. Cui, Biomaterials 32 (2011) 5551–5557.
[79] M.P. Mattson, R.C. Haddon, A.M. Rao, J. Mol. Neurosci. 14 (2000) 175–182.
[80] E.B. Malarkey, V. Parpura, Neurodegener. Dis. 4 (2007) 292–299.
[81] M. Yang, M. Zhang, Frontiers in Materials, 6, 2019.
[82] M. Chen, X. Qin, G. Zeng, Trends Biotechnol. 35 (2017) 836–846.
[83] J. Shin, Y. Yan, W. Bai, Y. Xue, P. Gamble, L. Tian, I. Kandela, C.R. Haney, W. Spees, Y. Lee, M. Choi, J. Ko, H. Ryu, J.-K. Chang, M. Pezhouh, S.-K. Kang, S. M. Won, K.J. Yu, J. Zhao, Y.K. Lee, M.R. MacEwan, S.-K. Song, Y. Huang, W.Z. Ray, J.A. Rogers, Nat. Biomed. Eng. 3 (2019) 37–46.
[84] E. González-Lavado, N. Iturrioz-Rodríguez, E. Padín-González, J. González, L. García-Hevia, J. Heuts, C. Pesquera, F. González, J.C. Villegas, R. Valiente, M. L. Fanarraga, Nanoscale 10 (2018) 11013–11020.
[85] C. Waugh, A. Blazevich, F. Fath, T. Korff, J. Anat. 220 (2012) 144–155.
[86] C.M. Boutry, A. Nguyen, Q.O. Lawal, A. Chortos, S. Rondeau-Gagné, Z. Bao, Adv. Mater. 27 (2015) 6954–6961.
[87] C.M. Boutry, Y. Kaizawa, B.C. Schroeder, A. Chortos, A. Legrand, Z. Wang, J. Chang, P. Fox, Z. Bao, Nat. Electron. 1 (2018) 314–321.